Shared Control Between Adaptive Autopilots and Human Operators for Anomaly Mitigation

Benjamin T. Thomsen * **Anuradha M. Annaswamy** *
Eugene Lavretsky **

* *Massachusetts Institute of Technology, Cambridge, MA 02139*
** *The Boeing Company, Huntington Beach, CA 92647*

Abstract: As aerial vehicles become more autonomous, and guidance and navigation systems become increasingly network-centric, there is a need to consider a swift response to the growing forms of anomalies that may occur in these systems. We introduce a shared decision-making and control framework between a human operator and an adaptive autopilot, where the human operator plays a supervisory role and the adaptive autopilot retains the responsibility for low-level regulation and command tracking tasks. The human operator provides key inputs based on a higher-level perception of the anomaly, such as an increased lag in response to command inputs, which are then used by the adaptive autopilot in a suitable manner. The resulting shared control architecture is demonstrated on an unmanned aerial vehicle, whose actuators abruptly change from first-order to second-order due to an anomaly.

Keywords: adaptive control, output feedback, anomaly detection and recovery, high relative degree, shared control

1. INTRODUCTION

In flight control systems, as in any complex dynamic system, uncertainties are inevitable. Uncertainties may occur for myriad reasons including modeling errors, environmental variations, unforeseen anomalies and disturbances, and of late, cyber attacks. The field of adaptive control (Narendra and Annaswamy (2005); Lavretsky and Wise (2013)) addresses a class of such uncertainties which are due to unknown parameters. By changing the control parameters online using a suitably constructed tracking error, the adaptive controller self-tunes its parameters and compensates for parametric uncertainties using online measurements. Recent advances in adaptive control have included the development of closed-loop reference models (CRMs) by Gibson et al. (2013), which greatly improves transient performance during online learning. While adaptive control is able to guarantee stability and tracking convergence in the presence of parametric uncertainties, other properties of the system – such as the order of a linear system – are assumed to be known *a priori* for control design.

Human operators of dynamical systems also develop mental models of expected plant behavior, often over long periods of active learning. Human pilots, for example, have been modeled and studied extensively to examine their use of information feedback and ability to adapt their control strategies to unfamiliar situations (see, for example, McRuer and Jex (1967); Phatak and Bekey (1969); Hess (2015); Zaal (2016)). In stressful situations, human pilots tend to apply high control gains, which coupled with certain dynamical anomalies may lead to pilot-induced oscillations and an increased risk of loss of control (Hess (1997)). Belcastro et al. (2014) found that the majority of transport aircraft loss of control incidents over a 15-year period involved inaction or improper action by the flight crew. Endsley (1996) points to pilot error following a transition from autonomous to manual control (often as the result of an anomaly) as a common factor in loss of control incidents. Issues with manual control of dynamical systems are exacerbated when the human operator is physically separated from the dynamics of the system, as is the case with remotely piloted vehicles (McCarley and Wickens (2004); Tvaryanas and Thompson (2008)). The additional complexities involved with remote operation include a lack of sensory and perceptive cues regarding the plant state and its environment, time delays between the plant and operator for both sensing and actuation, and difficulty ascertaining the open-loop dynamical response between control input and plant output (Lam et al. (2008)). The question then is whether one can combine both an adaptive control methodology and a remote human supervisor's decision-making and their complementary merits to mitigate the effects of severe anomalies in a more efficient manner. The design of such a shared control is the focus of this paper.

The results of this paper build on our earlier work on shared control architectures of adaptive autopilots and human pilots, reported in Farjadian et al. (2017) and Thomsen et al. (2018). Unlike these two papers, our focus here is on the case when only partial states are available as output measurements. In Section 2, the control problem investigated in this paper is described. Our explicit shared control solution to this problem is described in Section 3. The shared decision-making and control framework is

⋆ This work was supported by the Boeing Strategic University Initiative.

applied to the longitudinal control of high altitude, long endurance (HALE) unmanned aerial vehicles (UAVs) and simulated numerically in Section 4. We summarize the work in Section 5.

2. PROBLEM STATEMENT

We consider linear multi-input multi-output (MIMO) plant models of the form

$$\begin{aligned} \dot{x}_p &= (A_p + B_p\Theta_p^T)x_p + B_p\Lambda_p u_p \\ y_p &= C_p x_p, \qquad z_p = C_{pz}x_p \end{aligned} \tag{1}$$

where x_p is the plant state, u_p is the plant input, y_p is measured output, and z_p is regulated output. Uncertain dynamics lead to the introduction of unknown Θ_p and Λ_p in the plant model. It is assumed that the matrix CB has full rank, and thus the plant has uniform relative degree one (see Qu et al. (2016)). In addition to the dynamics (1), the plant's actuators are assumed to have dynamics that can be described as

$$\dot{u}_p + (D_1 + \Theta_1^T)u_p = D_1 u \tag{2}$$

where D_1 is a diagonal matrix representing nominal actuator parameters and Θ_1 models uncertainty in the actuator dynamics. The problem is to choose $u(t)$ such that $z_p(t)$ tracks an external command $z_{cmd}(t)$ as closely as possible.

The specific anomaly that we consider is assumed to introduce an abrupt change in actuator dynamics from (2) to the second-order model

$$\ddot{u}_p + (D_2 + \Theta_2^T)\dot{u}_p + (D_1 + \Theta_1^T)u_p = D_1 u \tag{3}$$

where in addition to Θ_1, Θ_2 is an unknown parameter as well. This change in dynamics means that the structure of the model used for control design is no longer accurate, and the autonomous controller may lose stability and command tracking ability. In particular, the challenge from the anomaly is the increase in relative degree between u and y_p from two to three.

In addition to an autonomous controller which generates control input $u(t)$ in (2) and (3), a human supervisor is tasked with the high-level operation of the plant (1), including mission and task planning (commanding its mode of operation) and monitoring to ensure safe and anomaly-free operation. In this paper, we consider remote human operation, an example of which is the supervision of multiple aerial vehicles, as illustrated in Fig. 1. It is assumed that the human supervisor has access to information on plant sensor measurements, state estimate, tracking performance, and health (via visual, haptic, and/or auditory interfaces), and is able to perceive changes in plant dynamics, such as an increased lag or decreased control effectiveness, via these interfaces. The problem we address is whether the design of $u(t)$ can be carried out using a shared decision-making and control architecture using both autonomous control methods and human operators so as to lead to a successful mitigation of an abrupt anomaly causing a change from (2) to (3) and restore tracking performance in the presence of uncertainty.

3. SHARED CONTROLLER

The shared control framework we propose is designed so as to combine the merits of both adaptive control algorithms and remote human operators. Adaptive autopilots (Lavretsky and Wise (2013)) allow for continuous autonomous operation of the vehicle in the presence of parametric uncertainties Θ_p, Λ_p, and Θ_1, while human operators supervise as necessary. We propose a shared controller to respond to an anomaly, which is assumed to change actuator dynamics from (2) to (3), by tasking the human operator with providing key inputs based on higher-level perception of the anomaly, and tasking the adaptive autopilot with retention of low-level regulation and command tracking tasks based on these inputs.

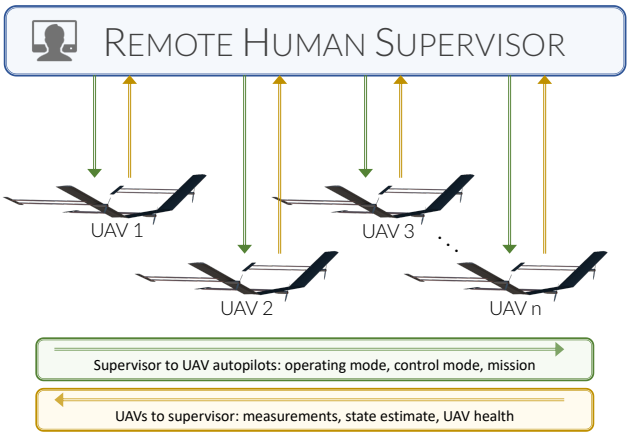

Fig. 1. Supervisory remote operation of HALE UAVs

In Section 3.1, we describe two adaptive autopilot designs, which, in combination with the human operator whose precise role is described subsequently in Section 3.2, will solve the problem presented in Section 2. The overall shared control architecture is summarized in Section 3.3.

3.1 Adaptive Output-Feedback Control

An autonomous controller is designed to track prescribed commands for plant outputs $z_p(t)$ in (1), and is described in detail in this section. To achieve the control goals stated in Section 2, our proposed autopilot includes two components:

(i) baseline control design using the robust servomechanism linear quadratic regulator method (RSLQR);
(ii) adaptive output-feedback augmentation for parametric uncertainties in the plant.

An additional integral error state is included as

$$e_z^{\mathcal{I}}(t) = \int_0^t \big(z_p(\tau) - z_{cmd}(\tau)\big)d\tau. \tag{4}$$

The augmented plant model with $x = \left[x_p^T \;\; x_{act}^T \;\; (e_z^{\mathcal{I}})^T\right]^T$ can written compactly as

$$\begin{aligned} \dot{x} &= \left(A + B_1\Psi_1^T + B_r\Psi_r^T\right)x + B_r\Lambda u + B_z z_{cmd} \\ y &= Cx, \qquad z = C_z x \end{aligned} \tag{5}$$

where $x \in \mathbb{R}^n$, $u \in \mathbb{R}^m$, $y \in \mathbb{R}^p$ are redefined states, inputs and outputs, respectively. This plant has unknown matrices Ψ_1, Ψ_r, and Λ, which contain plant uncertainties (Θ_p), actuator uncertainties (Θ_i in (2) and (3)), and control effectiveness (Λ_p), respectively. We restrict our attention in this paper to square plants with $m = p$. The

subscript r indicates the relative degree of the augmented plant, and the definitions of B_r and Ψ_r depend on whether the actuators are first-order (2) or second-order (3). It is noted that the augmented plant model which arises from the inclusion of actuator model (2) in the plant (1) has relative degree two, while the augmented plant model associated with the inclusion of actuator model (3) has relative degree three.

For control design, closed-loop reference models (Gibson et al. (2013)) are designed as

$$\dot{x}_m = A_m x_m + B_z z_{cmd} + L e_y + \mathcal{F}_r(t), \quad y_m = C x_m \quad (6)$$

where $e_y = y - y_m$, $A_m = A - B_r K^T$ with $K \in \mathbb{R}^{n\times m}$ is a baseline feedback control gain designed for the system without uncertainty using RSLQR, as described by Lavretsky and Wise (2013). L is a Luenberger-like residual feedback gain, and $\mathcal{F}_r(t)$ is a function used when $r \geq 2$ to recover stability properties in the presence of uncertainty.

We define a *nominal* adaptive autopilot for the plant (5) as one that successfully accommodates actuator dynamics in the form of (2) and unknown Θ_p, Θ_1, and Λ_p. We define a *recovery* adaptive autopilot to be one that is successful in accommodating actuator dynamics (3), i.e., when it is known that the relative degree is three, with uncertain parameters Θ_p, Θ_1, Θ_2, and Λ_p. For details of closed-loop stability guarantees with the nominal and recovery adaptive controllers, readers are referred to Qu et al. (2016) and Qu (2016), respectively. In what follows, a brief summary of these controllers is provided.

Nominal Adaptive Controller The control design for the plant with first-order actuator dynamics is summarized by providing definitions for CRM residual gain matrix L, function $\mathcal{F}_2(t)$, control law $u(t)$, and parameter adaptation. Note that B_2 represents B_r from (5) for this relative degree two plant.

The feedback matrix L is designed as follows. We define the "relative degree one input path"

$$B_1^a = \alpha_0 B_2 + \alpha_1 A B_2 \quad (7)$$

where $\alpha_i > 0$ are free design parameters. We then define

$$S = (C B_1^a)^T \quad (8)$$

$$\overline{C} = SC \quad (9)$$

$$R^{-1} = (\overline{C} B_1^a)^{-1}\big[\overline{C} A B_1^a + (\overline{C} A B_1^a)^T\big](\overline{C} B_1^a)^{-1} + \epsilon I \quad (10)$$

$$L = B_1^a R^{-1} S \quad (11)$$

where $\epsilon > 0$ (Qu et al. (2016)) is chosen to guarantee stability of the adaptive system.

The function $\mathcal{F}_2(t)$ makes use of scaled error signal

$$e_{sy}(t) = R^{-1} S e_y(t) \quad (12)$$

and a filtered version of this signal, $\overline{e}_{sy}(t)$, given in the form of a differential equation as

$$(\alpha_0 + \alpha_1 \frac{d}{dt})\big\{\overline{e}_{sy}(t)\big\} = \alpha_1 e_{sy}(t). \quad (13)$$

It is worth noting that this can be represented in the Laplace s-domain with a first-order filter

$$\overline{E}_{sy}(s) = \frac{\alpha_1}{\alpha_1 s + \alpha_0} E_{sy}(s).$$

$\mathcal{F}_2(t)$ is then defined as

$$\mathcal{F}_2(t) = B_2(\alpha_0 + \alpha_1 \frac{d}{dt})\big\{\hat{\Psi}_m^T(t)\bar{e}_{sy}(t)\big\} \quad (14)$$

where $\hat{\Psi}_m(t)$ is a matrix of adaptive parameters. Similar to (13), we define filtered reference model state, $\overline{x}_m(t)$, with the differential equation

$$(\alpha_0 + \alpha_1 \frac{d}{dt})\big\{\overline{x}_m(t)\big\} = \alpha_1 x_m(t). \quad (15)$$

We define a regressor vector of known signals as

$$\mathcal{X}(t) = \big[(K^T \overline{x}_m)^T, \quad x_m^T, \quad \overline{x}_m^T\big]^T. \quad (16)$$

The control law, $u(t)$, is then given by

$$u(t) = -(\alpha_0 + \alpha_1 \frac{d}{dt})\big\{\hat{\Psi}_\Lambda^T(t)\mathcal{X}(t)\big\} \quad (17)$$

where $\hat{\Psi}_\Lambda(t)$ is a matrix of adaptive parameters. The laws for adaptation of parameter matrices $\hat{\Psi}_m(t)$ and $\hat{\Psi}_\Lambda(t)$ are given by

$$\begin{aligned} \dot{\hat{\Psi}}_m(t) &= \Gamma_m \overline{e}_{sy}(t) e_y^T(t) S^T \\ \dot{\hat{\Psi}}_\Lambda(t) &= -\Gamma_\Lambda \mathcal{X}(t) e_y^T(t) S^T \end{aligned} \quad (18)$$

with diagonal adaptation gains Γ_m, $\Gamma_\Lambda > 0$. We note that the derivatives of the adaptive parameters, computed in (18), are used to implement (14) and (17) with the product rule of differentiation.

Recovery Adaptive Controller Control design with the second-order actuator model is similar to the nominal control design, but requires modifications to ensure strict positive realness of the transfer matrix of the model-following error dynamics.

The definition of L is modified by replacing B_1^a in (7) with

$$B_1^a = \alpha_0 B_3 + \alpha_1 A B_3 + \alpha_2 A^2 B_3 \quad (19)$$

and proceeding with (8)–(11). A definition for $\epsilon > 0$ in this case can be found in Qu (2016). To simplify notation, the operator $\Pi\{\cdot\}$ is defined as

$$\Pi\{\cdot\} = \big(\alpha_0 + \alpha_1 \frac{d}{dt} + \alpha_2 \frac{d^2}{dt^2}\big)\{\cdot\}. \quad (20)$$

The function $\mathcal{F}_3(t)$ utilizes filtered error vectors $\overline{e}_{sy}^{[1]}(t)$, $\overline{e}_{sy}^{[2]}(t)$, and $\overline{e}_{sy}^{[1][2]}(t)$, defined by the differential equations

$$\begin{aligned} \Pi\big\{\overline{e}_{sy}^{[1]}(t)\big\} &= (\alpha_1 + \alpha_2 \frac{d}{dt})\big\{e_{sy}(t)\big\} \\ \Pi\big\{\overline{e}_{sy}^{[2]}(t)\big\} &= \alpha_2 e_{sy}(t) \\ \Pi\big\{\overline{e}_{sy}^{[1][2]}(t)\big\} &= (\alpha_2 \frac{d}{dt})\big\{\hat{\phi}_1^T(t)\bar{e}_{sy}^{[1]}(t)\big\} \end{aligned} \quad (21)$$

where $e_{sy}(t)$ was defined in (12), $\hat{\phi}_1(t)$ is a vector of adaptive parameters, and coefficients $\alpha_i > 0$ are free design parameters. We define the integrated and scaled measurement output error,

$$e_y^{\mathcal{I}}(t) = \int_0^t L\big(y(\tau) - y_m(\tau)\big)d\tau \quad (22)$$

which is used to define filtered error signals $\overline{e}_{\mathcal{I}y}^{[1]}(t)$ and $\overline{e}_{\mathcal{I}y}^{[1][2]}(t)$, given by

$$\begin{aligned} \Pi\big\{\overline{e}_{\mathcal{I}y}^{[1]}(t)\big\} &= (\alpha_1 \frac{d}{dt} + \alpha_2 \frac{d^2}{dt^2})\big\{\hat{\Phi}_1^T(t) e_y^{\mathcal{I}}(t)\big\} \\ \Pi\big\{\overline{e}_{\mathcal{I}y}^{[1][2]}(t)\big\} &= (\alpha_2 \frac{d}{dt})\big\{\hat{\Lambda}^T(t)\overline{e}_{\mathcal{I}y}^{[1]}(t)\big\} \end{aligned} \quad (23)$$

where $\hat{\Phi}_1(t)$ and $\hat{\Lambda}(t)$ are matrices of adaptive parameters. We define operators

$$\begin{aligned} f_a\{\cdot\} &= \big(\alpha_0\alpha_2 B_3 + (\alpha_1 B_3 + \alpha_2 A B_3)\frac{d}{dt}\big)\{\cdot\} \\ f_b\{\cdot\} &= \alpha_2 B_3 \Pi\{\cdot\} \end{aligned} \tag{24}$$

and use these to define

$$\begin{aligned} \mathcal{F}_3(t) &= f_a\big\{\hat{\phi}_1^T(t)\overline{e}_{sy}^{[1]}(t) - \hat{\Lambda}^T(t)\overline{e}_{\mathcal{I}y}^{[1]}(t)\big\} \\ &+ f_b\big\{\hat{\phi}_1^T(t)\big[\overline{e}_{sy}^{[1][2]}(t) - \overline{e}_{\mathcal{I}y}^{[1][2]}(t)\big] + \hat{\phi}_2^T(t)\overline{e}_{sy}^{[2]}(t)\big\} \end{aligned} \tag{25}$$

where $\hat{\phi}_2(t)$ is an additional vector of adaptive parameters.

We define filtered reference model states $\overline{x}_m^{[1]}$ and $\overline{x}_m^{[2]}$ as

$$\begin{aligned} \Pi\big\{\overline{x}_m^{[1]}(t)\big\} &= (\alpha_1 + \alpha_2\frac{d}{dt})\big\{x_m(t)\big\} \\ \Pi\big\{\overline{x}_m^{[2]}(t)\big\} &= \alpha_2 x_m(t). \end{aligned} \tag{26}$$

Variable $\overline{v}_m(t)$ is introduced, with artificial time derivatives, such that

$$\begin{aligned} \overline{v}_m = x_m, \quad \frac{d}{dt}\{\overline{v}_m\} &= Ax_m + B_z z_{cmd} \\ \frac{d^2}{dt^2}\{\overline{v}_m\} &= A^2 x_m + AB_z z_{cmd} + B_z\frac{dz_{cmd}}{dt} - ALe_y. \end{aligned} \tag{27}$$

The regressor vector $\mathcal{X}(t)$ is redefined as

$$\mathcal{X}(t) = \big[(K^T\overline{x}_m^{[2]})^T, \quad \overline{v}_m^T, \quad \overline{x}_m^{[1]T}, \quad \overline{x}_m^{[2]T}\big]^T. \tag{28}$$

The control law $u(t)$ for the recovery controller is

$$\begin{aligned} u(t) = &-\Pi\big\{\hat{\Psi}^T(t)\mathcal{X}(t)\big\} \\ &-(\alpha_1\frac{d}{dt} + \alpha_2\frac{d^2}{dt^2})\big\{\hat{\Phi}_1^T(t)\big\}e_y^{\mathcal{I}}(t) \end{aligned} \tag{29}$$

where

$$\hat{\Psi}(t) = \big[\hat{\Upsilon}^T(t), \quad \hat{\Phi}_1^T(t), \quad \hat{\Phi}_2^T(t), \quad \hat{\Phi}_3^T(t)\big]^T \tag{30}$$

is a matrix of adaptive parameters.

In this controller, the adaptive parameters are adjusted using second-order tuners as in Qu (2016). We first define a regressor vector $\nu(t)$ of filtered error signals

$$\nu(t) = \Big[(\overline{e}_{\mathcal{I}y}^{[1][2]} - \overline{e}_{sy}^{[1]} - \overline{e}_{sy}^{[1][2]})^T, \quad (-\overline{e}_{sy}^{[2]})^T, \quad (\overline{e}_{\mathcal{I}y}^{[1]})^T\Big]^T \tag{31}$$

and associated matrix of adaptive parameters

$$\hat{\Theta}(t) = \big[\hat{\phi}_1^T(t), \quad \hat{\phi}_2^T(t), \quad \hat{\Lambda}^T(t)\big]^T. \tag{32}$$

Inputs to the second-order tuners are calculated by integrating

$$\begin{aligned} \dot{\hat{\Psi}}'(t) &= \Gamma_\Psi \mathcal{X} e_y^T S^T \mathrm{sgn}(\Lambda) \\ \dot{\hat{\Theta}}'(t) &= -\Gamma_\Theta \nu e_y^T S^T \end{aligned} \tag{33}$$

where $\Gamma_\Psi, \Gamma_\Theta > 0$ are diagonal adaptation gains.

The desired matrices of adaptive parameters are outputs of the tuners

$$\begin{aligned} \dot{X}_{\hat{\Psi}}(t) &= \big(A_T X_{\hat{\Psi}} + B_T(\hat{\Psi}'(t))^T\big)g(\mathcal{X}, \mu_{\mathcal{X}}) \\ \hat{\Psi}(t) &= (C_T X_{\hat{\Psi}})^T \\ \dot{X}_{\hat{\Theta}}(t) &= \big(A_T X_{\hat{\Theta}} + B_T(\hat{\Theta}'(t))^T\big)g(\nu, \mu_\nu) \\ \hat{\Theta}(t) &= (C_T X_{\hat{\Theta}})^T \end{aligned} \tag{34}$$

where

$$g(\mathbf{x}, \mu) = 1 + \mu\mathbf{x}^T\mathbf{x} \tag{35}$$

is a time-varying gain with scalar gain μ described in Qu (2016). $A_T \in \mathbb{R}^{2m\times 2m}$, $B_T \in \mathbb{R}^{2m\times m}$, and $C_T \in \mathbb{R}^{m\times 2m}$ are block diagonal matrices with diagonal blocks

$$A_{T,i} = \begin{bmatrix} 0 & 1 \\ -\frac{\alpha_0}{\alpha_2} & -\frac{\alpha_1}{\alpha_2} \end{bmatrix}, \quad B_{T,i} = \begin{bmatrix} 0 \\ \frac{\alpha_0}{\alpha_2} \end{bmatrix}, \quad C_{T,i} = [1\ 0] \tag{36}$$

Derivatives of the adaptive parameters, used in (21), (23), (25), and (29), are given by

$$\begin{aligned} \dot{\hat{\Psi}}(t) &= (C_T^\delta X_{\hat{\Psi}})^T, & \ddot{\hat{\Psi}}(t) &= (C_T^{\delta\delta} X_{\hat{\Psi}})^T \\ \dot{\hat{\Theta}}(t) &= (C_T^\delta X_{\hat{\Theta}})^T, & \ddot{\hat{\Theta}}(t) &= (C_T^{\delta\delta} X_{\hat{\Theta}})^T \end{aligned} \tag{37}$$

where $C_T^\delta, C_T^{\delta\delta} \in \mathbb{R}^{m\times 2m}$ are block diagonal matrices with diagonals $C_{T,i}^\delta = [0, \quad 1]$ and $C_{T,i}^{\delta\delta} = -\frac{1}{\alpha_2}[\alpha_0, \quad \alpha_1]$.

3.2 Human Supervisor

We task the remote human supervisor with the following three responsibilities for shared anomaly response.

Task 1. Timely detection of anomalous closed-loop dynamical behavior
Task 2. Isolation and characterization of anomaly
Task 3. Commanding a change from nominal autopilot (7)–(18) to recovery autopilot (19)–(37)

The first task requires an attentive human operator able to discern that

(a) an anomaly has occurred and control performance degradation is not caused solely by external disturbances;
(b) swift action must be taken in order to recover stability and performance;
(c) it may be possible to recover stability and performance via corrective action.

For the second task, the human operator must

(a) understand which control loop (e.g. pitch mode, roll mode, airspeed, in a fixed-wing UAV application) is affected by anomaly;
(b) perceive an increased lag in plant response to commands.

The final task for the trained remote human operator is the transfer of this diagnosis to the autopilot, by changing the relevant controller to its recovery mode.

3.3 Overall Shared Control Architecture

The shared control architecture between adaptive autopilots and a human operator that we propose is as follows. Before the occurrence of an anomaly, the nominal adaptive autopilot with control action defined in (17) is used to control the plant. An anomaly which abruptly changes actuator dynamics from (2) to (3) is assumed to occur at $t := t_1^*$. Following this time instant, the human operator is responsible for carrying out tasks 1–3 before the time limit at which failure would occur without action ($t := t_3^*$). The completion of task 3 by the human ($t := t_2^*$) results in a switch to the recovery adaptive autopilot with control action as in (29).

Note that our shared control architecture does not involve a handover of regulation and command tracking tasks to

the human following an anomaly. Instead, in our shared control architecture, the human operator is responsible for high-level cognition tasks while adaptive autopilots retain responsibility for low-level regulation, therefore directly leveraging and combining their complementary merits.

A detailed discussion of the stability of the closed-loop system with the overall shared controller is not carried out in this paper. But it is clear that if the human completes tasks 1–3 sufficiently fast (i.e., $t_2^* < t_3^*$), then the shared controller will guarantee boundedness of the closed-loop system and convergence of $e(t) = x(t) - x_m(t)$ to zero if our assumptions are satisfied. We carry out a detailed simulation study in the following section and evaluate the performance of the shared controller proposed above.

4. ANOMALY RESPONSE SIMULATIONS

The shared control solution introduced in Section 3 is applied to the problem introduced in Section 2 on a high altitude, long endurance (HALE) model. HALE aerial platforms, such as the solar-electric NASA/AeroVironment Helios and Facebook Aquila, have unique design considerations to satisfy goals of uninterrupted weeks- or months-long operation. To reduce power draw, HALE aircraft designs save mass by allowing wings to bend, and may be classified as very flexible aircraft (VFA). Compared to typical fixed-wing aircraft, these aircraft operate at low speed, and may use low-bandwidth actuators which must be accounted for in control design. HALE VFA platforms are likely to have significant modeling uncertainties and online variation in dynamics due to flexible effects and degradation over long-term operation. It is assumed that these vehicles are assumed to be unmanned and that they require supervision from remote human operators as needed.

The aircraft model used in simulation, developed by Gibson et al. (2011) for longitudinal control design applications, is rendered in Figure 2 and described in Section 4.1. The results of numerical simulations on the control and anomaly recovery with this MIMO plant are then presented in Section 4.2, comparing the shared anomaly response to alternative anomaly responses.

4.1 Aircraft Model

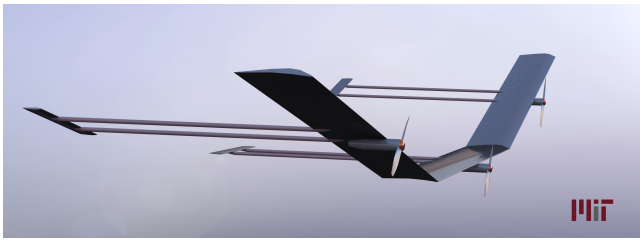

Fig. 2. Rendering of very flexible aircraft model

The aircraft model represents the nonlinear longitudinal dynamics of a HALE VFA concept with three rigid lifting sections, hinged together such that the aircraft is able to bend at the joints of the three sections. The pitch mode dynamics of this nonlinear model is defined by the state vector

$$x_{\text{vfa}} = \begin{bmatrix} V \\ \alpha \\ h \\ \theta \\ q \\ \eta \\ \dot{\eta} \end{bmatrix} = \begin{bmatrix} \text{Airspeed (ft/s)} \\ \text{Angle of attack (rad)} \\ \text{Altitude (ft)} \\ \text{Pitch angle (rad)} \\ \text{Pitch rate (rad/s)} \\ \text{Dihedral (rad)} \\ \text{Dihedral rate (rad/s)} \end{bmatrix} \tag{38}$$

We linearize and trim the aircraft in straight and level flight using the inputs

$$u_{\text{vfa}} = \begin{bmatrix} \delta_{th} \\ \delta_{a,c} \\ \delta_{a,o} \\ \delta_{e,c} \\ \delta_{e,o} \end{bmatrix} = \begin{bmatrix} \text{Thrust (lbf)} \\ \text{Center aileron (rad)} \\ \text{Outer aileron (rad)} \\ \text{Center elevator (rad)} \\ \text{Outer elevator (rad)} \end{bmatrix} \tag{39}$$

Assuming small deviations in altitude, the state vector corresponding to (1) is

$$x_p = [V \quad \alpha \quad \theta \quad q \quad \eta \quad \dot{\eta}]^T . \tag{40}$$

We consider the control task of tracking commands for the dihedral angle and vertical acceleration, using control inputs $\delta_{a,o}$ and $\delta_{e,c}$ only, so the vector u_p in (1) is

$$u_p = [\delta_{a,o} \quad \delta_{e,c}]^T . \tag{41}$$

Regulation of the dihedral angle is desired, as a large dihedral angle is inefficient for lift generation and introduces instability in the open-loop dynamics, while a small dihedral angle will require more control effort to hold, increasing drag and power requirements and imparting twisting moments on the aircraft.

The measurements available for control design are the pitch rate, dihedral angle, and vertical acceleration, leading to plant outputs

$$\begin{aligned} y_p &= \begin{bmatrix} q \end{bmatrix} = \begin{bmatrix} \text{Pitch rate (rad/s)} \end{bmatrix} \\ z_p &= \begin{bmatrix} \eta \\ A_z \end{bmatrix} = \begin{bmatrix} \text{Dihedral angle (rad)} \\ \text{Vertical acceleration (ft/s)} \end{bmatrix} \end{aligned} \tag{42}$$

and the outputs for the augmented plant (5),

$$y = \begin{bmatrix} q \\ \int z_p - z_{cmd} \end{bmatrix}, \quad z = z_p. \tag{43}$$

For numerical simulations, the VFA model is trimmed at an airspeed of 68 ft/s, altitude of 40,000 ft, 2.8° angle of attack and pitch angle (level flight), and dihedral angles ranging from 0 to 20° in 1° increments. Figure 3 shows pole locations of the linearized plant for different dihedral angles, and Figure 4 shows instability of the linearized plant when trimmed above 11° dihedral. Figure 5 shows the thrust and control surface deflections for the trimmed VFA model over a range of dihedral angles.

The plant is augmented with a linear actuator model corresponding to (2) in the nominal case and (3) following an anomaly. The vehicle simulation with first-order actuators (2) uses parameters

$$D_1 = 2I_2, \quad \Theta_1 = -1.5I_2 \tag{44}$$

where Θ_1 is assumed to be unknown for control design, and I_2 is the 2×2 identity matrix.

Simulation of the anomalous dynamics (3) uses second-order actuators with parameters

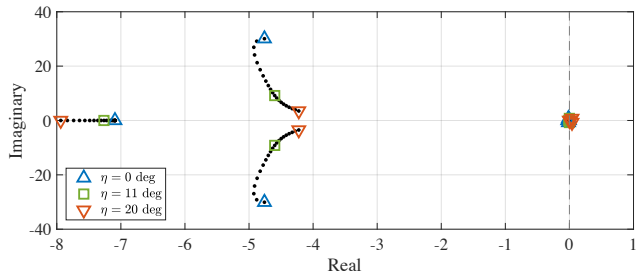

Fig. 3. Poles of linearized system for different dihedral angles

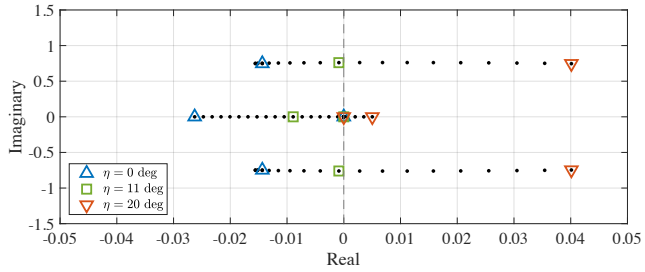

Fig. 4. Dominant poles of linearized system, which move into the right-half complex plane when $\eta > 11°$

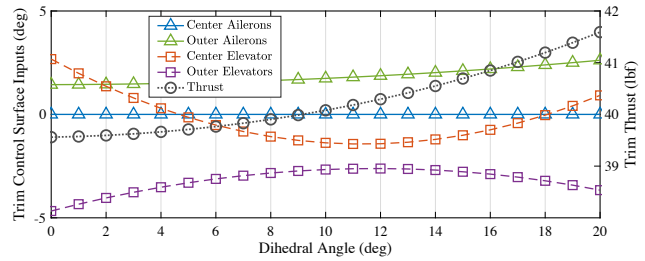

Fig. 5. Actuator trim at different dihedral angles

$$\begin{bmatrix} D_1 \\ D_2 \end{bmatrix} = \begin{bmatrix} 4I_2 \\ 2.8I_2 \end{bmatrix}, \quad \begin{bmatrix} \Theta_1 \\ \Theta_2 \end{bmatrix} = \begin{bmatrix} -3.75I_2 \\ -2I_2 \end{bmatrix} \tag{45}$$

where Θ_1 and Θ_2 are assumed to be unknown for the adaptive control design. Matrices Θ_p and Λ_p used in simulation represent modeling errors that are assumed to be caused by linearization of the VFA model at an incorrect dihedral angle, and an 80% reduction in actuator effectiveness, respectively, and are given by

$$\Theta_p^T = \begin{bmatrix} 0.6 & -4.52 & 0 & 0.05 & 0.41 & 1.47 \\ 0.1 & 1.83 & 0 & -0.02 & -0.35 & -0.59 \end{bmatrix}$$
$$\Lambda_p = 0.2I_2. \tag{46}$$

The structural design of the HALE VFA is assumed to be such that it can withstand an anomaly with the nominal control design for about $360s$ ($t_3^* - t_1^* \sim 360s$), while the human operator is assumed to perceive the abrupt increase in lag in the VFA's response to commands, and thus the increase in relative degree, within $200s$ ($t_2^* - t_1^* \sim 200s$).

Both the nominal and recovery adaptive controllers utilize a number of free design parameters, including LQR weight matrices and adaptation rates. Their numerical values in the simulations presented here are available online [1] .

[1] `http://aaclab.mit.edu/resources/cphs-2018/`

4.2 Numerical Simulations and Results

We begin by simulating the HALE VFA under nominal autonomous control, responding to step inputs in commands for the dihedral angle and vertical acceleration, with the following three variants.

Nom-1 Baseline RSLQR without uncertainty in control model ($\Theta_p = 0$, $\Lambda_p = 0$, $\Theta_1 = 0$)

Nom-2 Baseline RSLQR with uncertainty in control model (Θ_1 in (44); Θ_p, Λ_p in (46))

Nom-3 Baseline RSLQR + adaptive control with uncertainty in control model (Θ_1 in (44); Θ_p, Λ_p in (46))

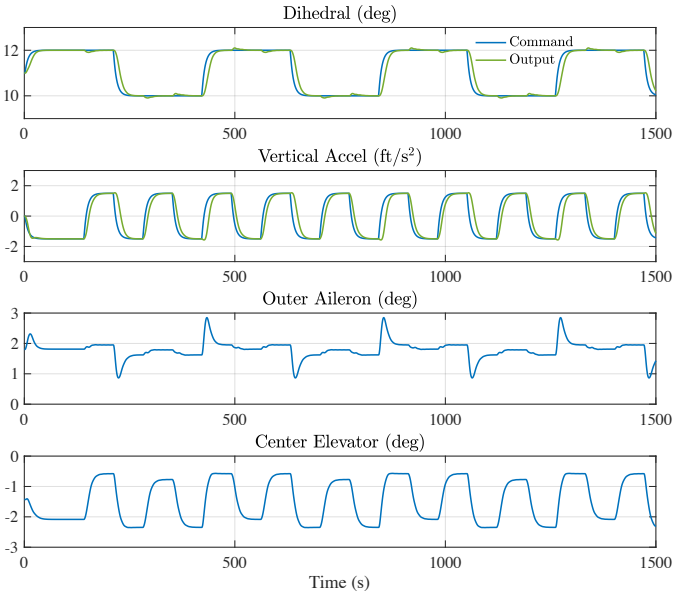

Fig. 6. Nom-1 simulation: RSLQR with no uncertainty in the control model

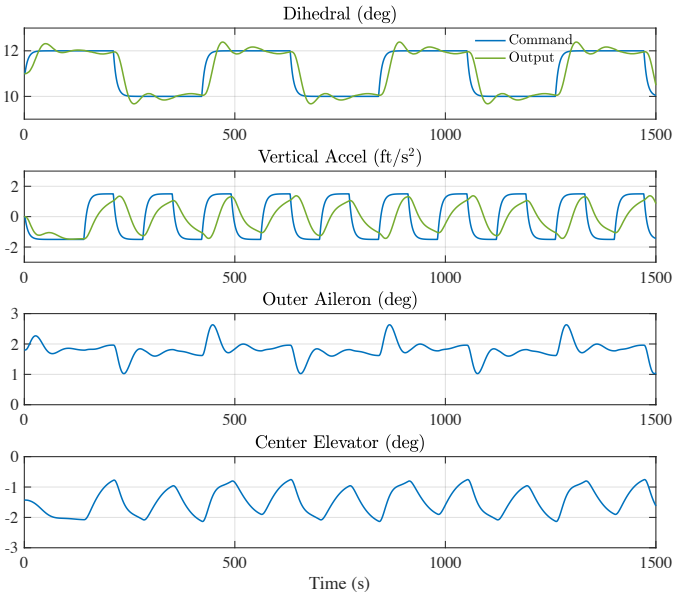

Fig. 7. Nom-2 simulation: RSLQR with uncertainties Θ_p, Λ_p, and Θ_1

These simulations, presented in Figs. 6, 7, and 8 respectively, show how the adaptive controller with output feedback described in (7)–(18) is able to recover the desired

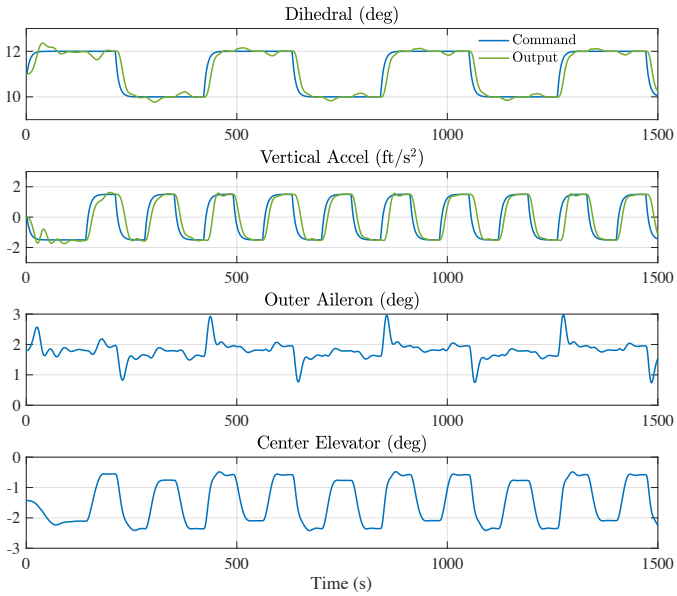

Fig. 8. Nom-3 simulation: RSLQR + adaptive control with uncertainties Θ_p, Λ_p, and Θ_1

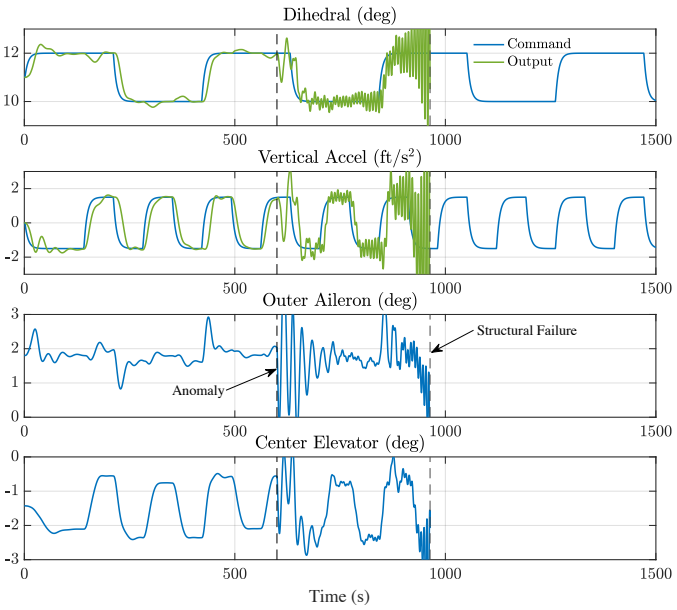

Fig. 9. AR-1 simulation: passive response to dynamical anomaly results in structural failure after 6 minutes

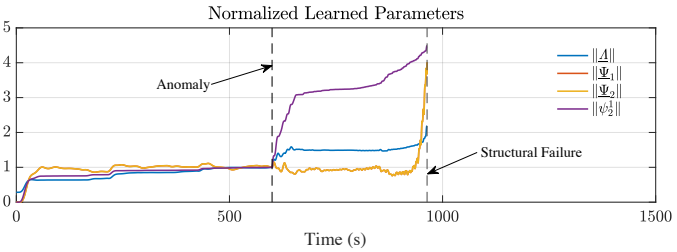

Fig. 10. AR-1 simulation: adaptive parameters diverge as controller struggles to adapt to unmodeled dynamics

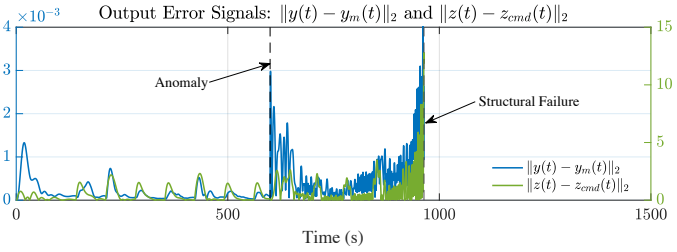

Fig. 11. AR-1 simulation: model-following output error and command tracking error grow after anomaly

closed-loop performance with uncertainty in plant and actuator parameters, which are assumed to be present due to modeling errors. With the baseline RSLQR controller only, the system suffers degraded command tracking performance in the presence of uncertainty (Fig. 7), especially for vertical acceleration tracking.

In what follows, we simulate the introduction of an anomaly into the dynamics, causing the vehicle's actuators to change abruptly from the uncertain first-order dynamics (2) to the uncertain second-order dynamics (3) at $t_1^* = 600s$. We consider three responses to the anomaly.

AR-1 (Passive) The nominal autopilot retains control without intervention from the human supervisor

AR-2 (Manual) The human operator takes over manual control of the affected vehicle

AR-3 (Shared) Responsibilities are shared between the human and autopilot as described in Section 3

Figs. 9–11 show the result of a passive response (AR-1) in which the human operator ignores vehicle performance degradation and allows the nominal adaptive controller to continue operating on the plant with anomalous dynamics. The closed-loop system loses stability, leading to oscillations in vehicle output and eventual structural failure of the VFA at $t_3^* = 960s$. Note that a passive response using only the RSLQR controller (no adaptation) also leads to structural failure following the anomaly.

Numerical simulations of the AR-2 response (purely manual control) are not carried out, as they are not deterministic and require high-fidelity human-in-the-loop experiments to characterize. The limitations of such a response are discussed in more detail elsewhere (e.g. Endsley (1996); Hess (2015)).

Results of the AR-3 (shared control) anomaly response simulation are shown in Figs. 12–14. After the anomaly is introduced at $t_1^* = 600s$, the nominal adaptive controller attempts to control the system whose dynamics are not fully accounted for in the control model. Simultaneously in the shared control framework, the human operator notices the anomalous closed-loop control behavior, and via an interface switches the controller to the higher relative degree design (19)–(37) at $t_2^* = 800s$, which is the culmination of the human operator's action. For $t \geq t_2^*$, the vehicle remains under autonomous control with the recovery adaptive controller and is able to reestablish nominal command tracking performance and avert failure (which was assumed to occur at $t_3^* = 960s$ with AR-1).

5. SUMMARY

This work develops a shared control framework between adaptive autopilots and remote human operators of aerial vehicles. The autonomous control design builds on two

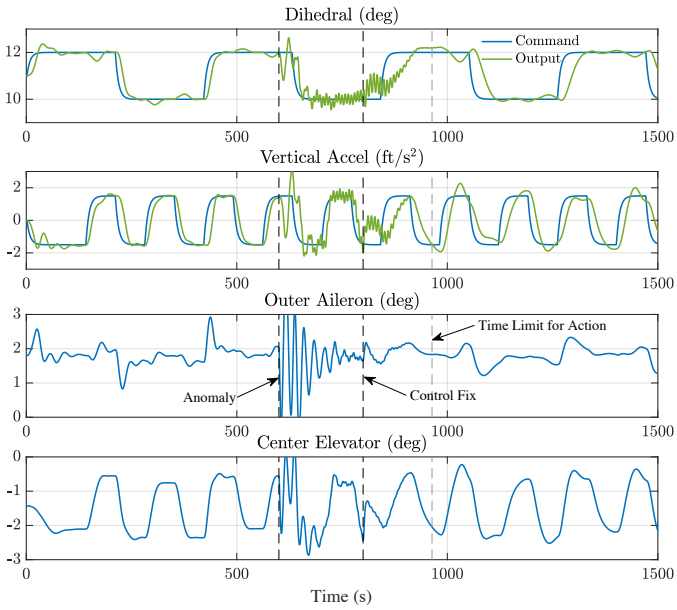

Fig. 12. AR-3 simulation: shared response to the dynamical anomaly results in recovery of vehicle performance

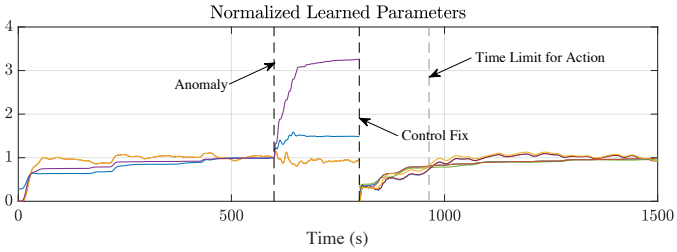

Fig. 13. AR-3 simulation: the change in control model at $t_2^* = 800s$ stops the divergence of adaptive parameters

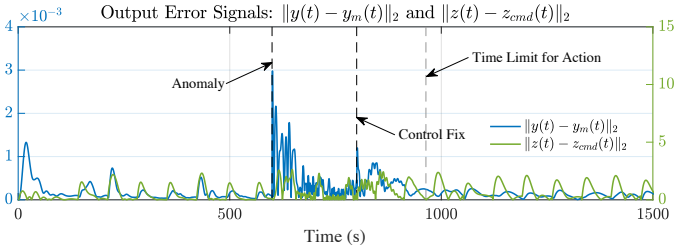

Fig. 14. AR-3 simulation: the change in control model at $t_2^* = 800s$ returns error signals to nominal levels

recent advances in adaptive control theory, namely the use of closed-loop reference models for improved transient performance, and computationally efficient control designs for output-feedback systems having relative degree two or greater. In our shared response to dynamical anomalies, the human operator provides key inputs based on a higher-level perception of the anomaly, and these inputs are used by the adaptive autopilot retaining responsibility for low-level regulation and command tracking tasks. The shared control response is demonstrated in simulation on the longitudinal dynamics of an unmanned HALE VFA model.

REFERENCES

Belcastro, C.M., Foster, J., Newman, R.L., Groff, L., Crider, D.A., and Klyde, D.H. (2014). Preliminary analysis of aircraft loss of control accidents: Worst case precursor combinations and temporal sequencing. In *AIAA Guidance, Navigation, and Control Conference*, 10.2514/6.2014–0612.

Endsley, M.R. (1996). Automation and situation awareness. In R. Parasuraman and M. Mouloua (eds.), *Automation and Human Performance: Theory and Applications*, 163–181. Lawrence Erlbaum.

Farjadian, A.B., Annaswamy, A.M., and Woods, D. (2017). Bumpless reengagement using shared control between human pilot and adaptive autopilot. In *IFAC World Congress*, 5343–5348. IFAC.

Gibson, T., Annaswamy, A.M., and Lavretsky, E. (2011). Modeling for control of very flexible aircraft. In *AIAA Guidance, Navigation, and Control Conference*, 10.2514/6.2011–6202. doi:10.2514/6.2011-6202.

Gibson, T.E., Annaswamy, A.M., and Lavretsky, E. (2013). On adaptive control with closed-loop reference models: Transients, oscillations, and peaking. *IEEE Access*, 1, 703–717.

Hess, R.A. (1997). Unified theory for aircraft handling qualities and adverse aircraft-pilot coupling. *Journal of Guidance, Control, and Dynamics*, 20(6), 1141–1148.

Hess, R.A. (2015). Modeling human pilot adaptation to flight control anomalies and changing task demands. *Journal of Guidance, Control, and Dynamics*, 38(6), 655–666.

Lam, T., Mulder, M., and Van Paassen, M. (2008). Haptic feedback in uninhabited aerial vehicle teleoperation with time delay. *Journal of Guidance, Control, and Dynamics*, 31(6), 1728–1739.

Lavretsky, E. and Wise, K.A. (2013). *Robust and Adaptive Control with Aerospace Applications*. Springer.

McCarley, J.S. and Wickens, C.D. (2004). Human factors concerns in UAV flight.

McRuer, D.T. and Jex, H.R. (1967). A review of quasi-linear pilot models. *IEEE Transactions on Human Factors in Electronics*, (3), 231–249.

Narendra, K.S. and Annaswamy, A.M. (2005). *Stable Adaptive Systems*. Dover Publications.

Phatak, A.V. and Bekey, G.A. (1969). Model of the adaptive behavior of the human operator in response to a sudden change in the control situation. *IEEE Transactions on Man-Machine Systems*, 10(3), 72–80.

Qu, Z. (2016). *Adaptive Output-Feedback Control and Applications to Very Flexible Aircraft*. Ph.D. thesis, Massachusetts Institute of Technology.

Qu, Z., Annaswamy, A.M., and Lavretsky, E. (2016). Adaptive output-feedback control for a class of multi-input-multi-output plants with applications to very flexible aircraft. In *American Control Conference (ACC), 2016*, 1613–1618. IEEE.

Thomsen, B.T., Annaswamy, A.M., and Lavretsky, E. (2018). Shared control between human and adaptive autopilots. In *AIAA Guidance, Navigation, and Control Conference*, 10.2514/6.2018–1574.

Tvaryanas, A.P. and Thompson, W.T. (2008). Recurrent error pathways in hfacs data: Analysis of 95 mishaps with remotely piloted aircraft. *Aviation, Space, and Environmental Medicine*, 79(5), 525–532.

Zaal, P.M. (2016). Manual control adaptation to changing vehicle dynamics in roll–pitch control tasks. *Journal of Guidance, Control, and Dynamics*, 1046–1058.